

# Supplementary material for: Ensemble projections elucidate effects of uncertainty in nitrogen limitation on future terrestrial carbon uptake

Johannes Meyerholt<sup>1,2,†</sup>, Kerstin Sickel<sup>1</sup>, and Sönke Zaehle<sup>1,3</sup>

<sup>1</sup>Biogeochemical Integration Department, Max Planck Institute for Biogeochemistry, Hans-Knöll-Str. 10, Jena, 07745, Germany

<sup>2</sup>International Max-Planck Research School Global Biogeochemical Cycles, Hans-Knöll-Str. 10, Jena, 07745, Germany

<sup>3</sup>Michael Stifel Center Jena for Data-driven and Simulation Science, Ernst-Abbe-Platz 2, Jena, 07743, Germany

†deceased

**Correspondence:** Sönke Zaehle (szaehle@bgc-jena.mpg.de)

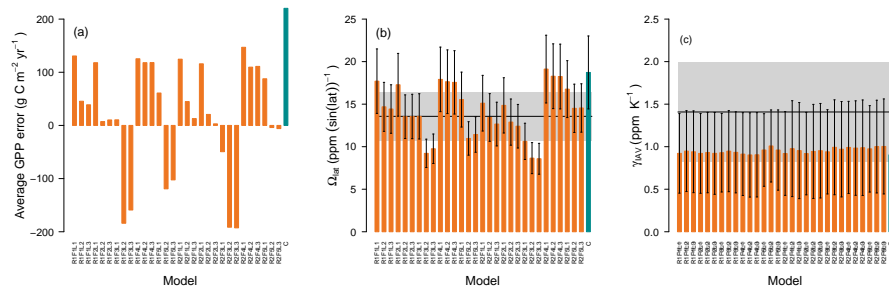


**Figure S1.** Supplement to Fig. 2 with individual model results instead of model groups. (A) Average error between model predictions and observational estimate (Jung et al., 2011) of gross primary productivity (GPP), averaged over the years 1982-2011 and the 40°N to 80°N latitudes. Individual models are identified by the algorithms active for C:N ratio flexibility, BNF, and nitrogen loss, with "C" indicating the carbon-only reference simulation. (B) Modeled gradients of the average 1982-2011 northern hemispheric seasonal CO<sub>2</sub> amplitude ( $\Omega_{\text{lat}}$ ). Bars indicate model results, black line shows the observational estimate. Error bars and shaded area indicate the average error between the line fit (Fig. 1C) and the measurements or model results at the respective CO<sub>2</sub> measurement stations (Tab. S2). (C) Comparison of modelled and measurement-based (black line and shaded area) 1982-2011 sensitivities of interannual CO<sub>2</sub> growth rate anomalies to changes in global temperatures  $\gamma_{\text{IAG}}$ . For simulations and measurements, the error bars and the shaded area indicate the error in  $\gamma_{\text{IAG}}$  over the 30 year time span. Individual models are identified by the algorithms active for C:N ratio flexibility, BNF, and nitrogen loss, with "C" indicating the carbon-only reference simulation.

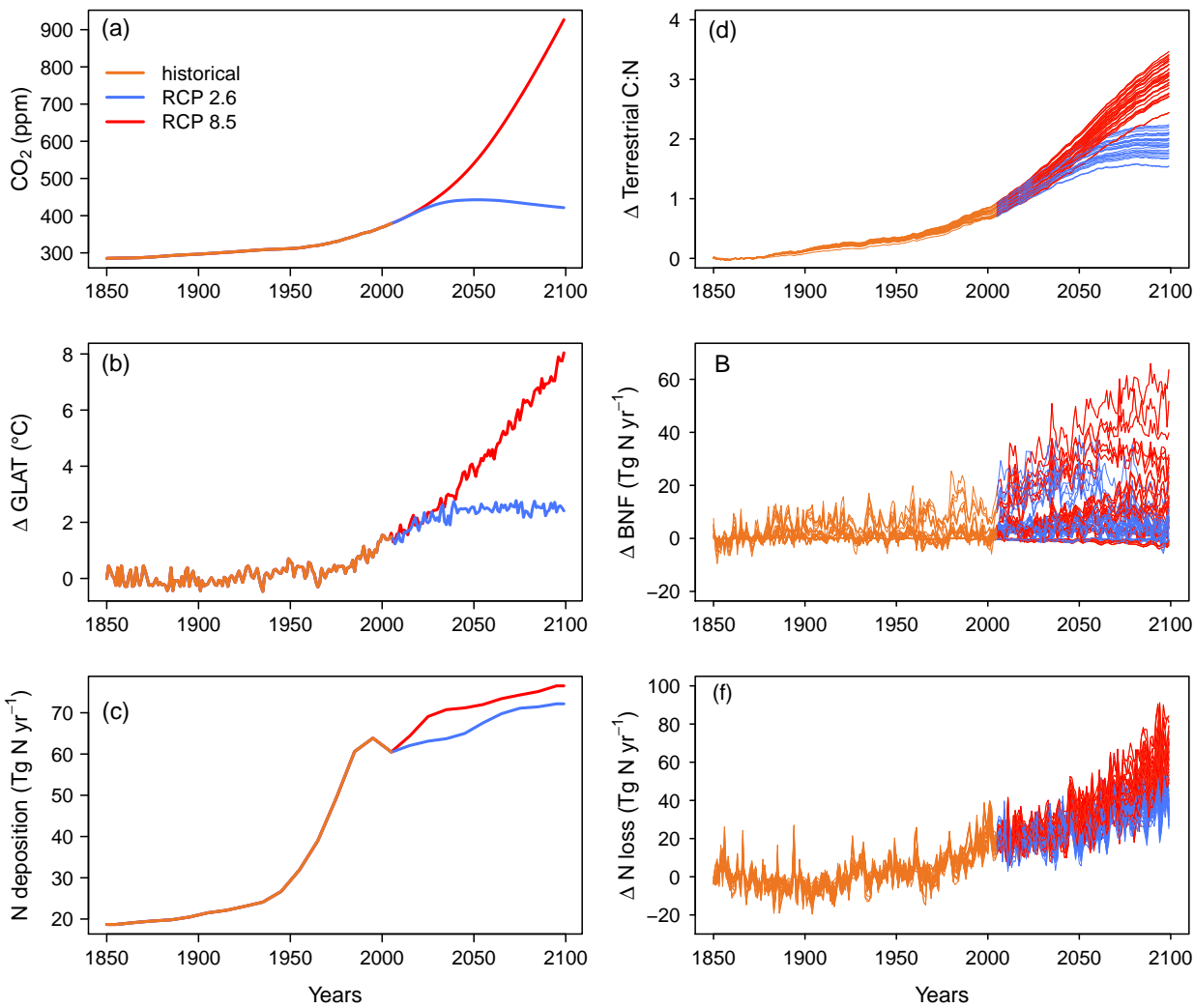


**Figure S2.** Globally integrated drivers of the simulations ((a) CO<sub>2</sub>, (b) global land air temperature (GLAT) and (c) N deposition over land) as well as simulated changes in (d) total ecosystem C:N ratios, (e) biological nitrogen fixation (BNF), and (f) nitrogen loss (1850-2099). Changes in biosphere are presented relative to the averages over the 1850-1880 period. Shown are simulation results from all 30 members of the carbon-nitrogen model ensemble over the common historical period (1850-2005), as well as the scenario periods (2006-2099) for RCP 2.6 and RCP 8.5.

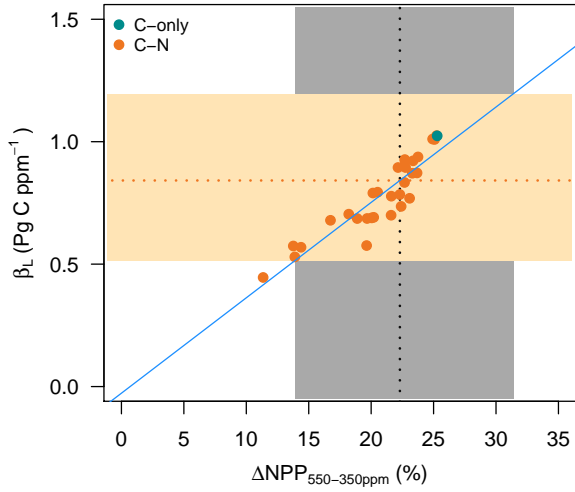


**Figure S3.** Modeled sensitivity of land carbon storage to increasing atmospheric CO<sub>2</sub> concentrations in dependence on the productivity response to increasing atmospheric CO<sub>2</sub> concentrations.  $\Delta NPP_{550-350\text{ppm}}$  indicates the relative change in global average net primary productivity (NPP) in response to the gradual increase in atmospheric CO<sub>2</sub> concentrations from 350 ppm (year 1988; taken as the 1983-1992 mean) to 550 ppm (year 2052; taken as the 2047-2056 mean). Here,  $\beta_L$  indicates the sensitivity of global land carbon storage to the same perturbation. The black dotted line and grey area indicate the range of observations of plant productivity responses to a CO<sub>2</sub> concentration increase of 200 ppm (2). The blue line indicates the linear fit for the relationship. The overlap of this fit with the observational range of  $\Delta NPP_{550-350\text{ppm}}$  determines the range of probable model estimates for  $\beta_L$  (orange dotted line and area).

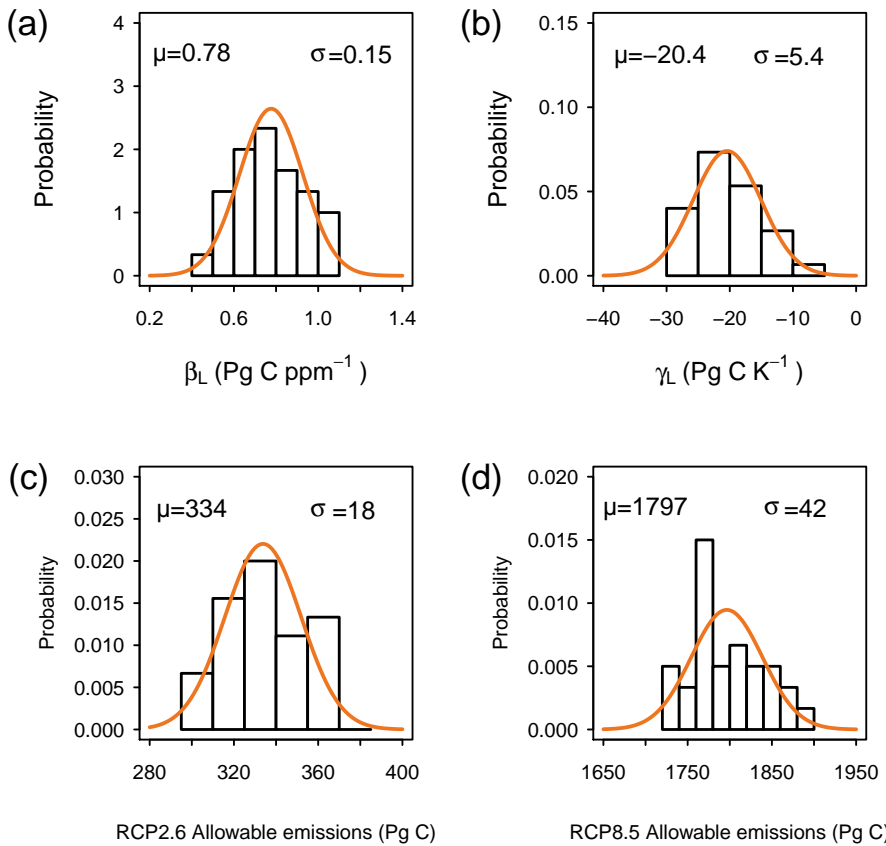


**Figure S4.** Gauss functions (orange) used to approximate the unconstrained distributions of model ensemble predictions (black) of carbon cycle feedbacks (1850-2099) and RCP-compatible anthropogenic carbon emissions (2006-2099). Distributions of predictions for (a) the carbon-concentration feedback parameter  $\beta_L$ , (b) the carbon-climate feedback parameter  $\gamma_L$ , as well as the (c) RCP2.6 and (d) RCP8.5 compatible anthropogenic carbon emissions.  $\mu$ , mean;  $\sigma$ , standard deviation.

## 1 Weighting of model results according to atmospheric constraints

For each pairing of model prediction and observed benchmark, we performed an ANOVA analysis to determine a p-value, formally quantifying the level of statistical significance of the model prediction of  $\Omega_{\text{lat}}$  compared with the observed atmospheric data (Table A2). We then divided each p-value by the sum of all p-values (one for each model version) and used the 5 results as relative weights for each model prediction. In Fig. 9, we present the distribution of model predictions for feedback parameters and allowable emissions as probability densities. For the unconstrained ensemble, we used the mean ( $\mu$ ) and SD (SD) of the ensemble predictions to approximate these distributions as symmetrical Gauss distributions (Fig. S4) according to

the established formula:

$$p(x) = \frac{1}{\sigma\sqrt{2\pi}} e^{-\frac{1}{2}(\frac{x-\mu}{\sigma})^2} \quad (\text{S1})$$

- 10 where  $p(x)$  is the relative probability for the model result of value  $x$ . To obtain the constrained mean of predictions  $\mu^*$ , we calculated a weighted mean that uses the  $p$ -values established above as relative weights  $w_i$  ( $\sum w_i = 1$ ):

$$\mu^* = \sum w_i \times x_i \quad (\text{S2})$$

where  $x_i$  denotes the model result corresponding to the weight  $w_i$ , and . We then applied the weights to determine the weighted standard deviation  $\sigma^*$  for the constrained distribution:

$$15 \quad \sigma^* = \sqrt{\sum w_i(x_i - \mu^*)^2} \quad (\text{S3})$$

We then used  $\mu^*$  and  $\sigma^*$  with SI Appendix, Eq. S1 to obtain the constrained distributions (blue curves in Fig. 9).

Table S1. Average simulated reservoir sizes and flux magnitudes for key global carbon and nitrogen properties (1996-2005).

Model	C <sub>land</sub> Pg C	C <sub>veg</sub> Pg C	C <sub>soil</sub> Pg C	N <sub>land</sub> Pg N	C <sub>veg</sub> Pg N	N <sub>soil</sub> Pg N	GPP PgCyr <sup>-1</sup>	NPP PgCyr <sup>-1</sup>	R <sub>a</sub> + R <sub>b</sub> PgCyr <sup>-1</sup>	fN <sub>anthr.</sub> PgNyr <sup>-1</sup>	BNF PgNyr <sup>-1</sup>	fN <sub>loss</sub> PgNyr <sup>-1</sup>	fN <sub>up</sub> PgNyr <sup>-1</sup>	fN <sub>min</sub> PgNyr <sup>-1</sup>
R1F1L1	1760	518	1243	98	3.675	95	128	60	127	0.13	0.117	0.23	1.03	1.002
R1F1L2	1701	506	1195	98	3.66	94	127	59	126	0.13	0.116	0.227	1.022	0.991
R1F1L3	1702	507	1195	97	3.669	93	127	59	126	0.13	0.116	0.223	1.022	0.988
R1F2L1	1752	515	1237	98	3.65	94	128	60	126	0.13	0.096	0.209	0.929	0.994
R1F2L2	1675	501	1175	95	3.608	91	126	59	125	0.13	0.094	0.201	0.917	0.976
R1F2L3	1684	505	1180	95	3.637	91	126	59	125	0.13	0.093	0.199	0.918	0.975
R1F3L1	1655	506	1149	91	3.56	87	124	58	123	0.13	0.099	0.212	0.883	0.952
R1F3L2	1531	481	1050	86	3.459	82	121	56	120	0.13	0.097	0.204	0.859	0.921
R1F3L3	1564	489	1075	87	3.51	83	122	56	121	0.13	0.097	0.203	0.867	0.928
R1F4L1	1759	515	1244	97	3.615	94	128	60	126	0.13	0.065	0.172	0.961	0.993
R1F4L2	1761	513	1248	98	3.624	95	128	60	127	0.13	0.048	0.151	0.985	0.995
R1F4L3	1767	515	1252	99	3.654	95	128	60	127	0.13	0.037	0.139	1.001	0.998
R1F5L1	1686	502	1184	93	3.51	89	125	58	123	0.13	0.075	0.186	0.911	0.957
R1F5L2	1546	474	1072	87	3.375	83	121	56	120	0.13	0.063	0.169	0.895	0.924
R1F5L3	1587	488	1099	88	3.48	84	123	57	122	0.13	0.057	0.163	0.916	0.939
R2F1L1	1787	497	1290	108	3.476	104	140	61	139	0.13	0.115	0.228	1.142	1.112
R2F1L2	1732	459	1273	112	4.03	108	149	60	147	0.13	0.114	0.221	1.304	1.269
R2F1L3	1723	461	1263	111	3.985	107	148	60	146	0.13	0.114	0.218	1.298	1.261
R2F2L1	1774	492	1282	106	3.351	103	139	61	137	0.13	0.096	0.207	1.033	1.095
R2F2L2	1725	460	1265	109	3.915	104	147	60	145	0.13	0.093	0.195	1.182	1.233
R2F2L3	1726	464	1262	108	3.924	104	147	60	145	0.13	0.092	0.194	1.191	1.241
R2F3L1	1654	471	1184	99	3.389	95	136	58	135	0.13	0.103	0.214	1.004	1.072
R2F3L2	1580	430	1150	100	3.871	96	142	57	141	0.13	0.101	0.204	1.145	1.206
R2F3L3	1597	435	1162	101	3.875	97	143	57	141	0.13	0.101	0.203	1.156	1.216
R2F4L1	1905	492	1413	119	3.453	116	137	69	135	0.13	0.092	0.195	1.218	1.268
R2F4L2	1880	489	1391	117	3.568	113	139	68	137	0.13	0.07	0.168	1.263	1.283
R2F4L3	1893	490	1403	119	3.646	115	141	69	139	0.13	0.056	0.152	1.326	1.329
R2F5L1	1892	496	1396	114	3.403	110	135	67	133	0.13	0.092	0.2	1.175	1.23
R2F5L2	1886	485	1401	113	3.707	109	138	66	136	0.13	0.078	0.178	1.237	1.271
R2F5L3	1907	483	1423	116	3.802	112	141	67	139	0.13	0.072	0.169	1.322	1.348
Ens. mean	1726	488	1239	102	3.636	98	133	61	132	0.13	0.089	0.193	1.07	1.1
Ens. SD	110	23	105	10	0.187	10	9	4	9	0.00	0.022	0.055	0.153	0.145
C-only	1857	518	1339	112	4.061	107	138	62	136	0.13	0.116	0.291	1.08	1.052

**Table S2.** Statistical measures for the performed regression analyses (Fig. 1a and b; 7; S1), where p-values are the result of an ANOVA testing whether or not the regression slopes derived from the simulations are significantly different to the regression slopes derived from the observations.

Model/Observation	R <sup>2</sup> <sub>seas.</sub>	Ω <sub>lat</sub> intercept (ppm)	Ω <sub>lat</sub> slope ( $\frac{\text{ppm}}{\sin(\text{lat})}$ )	Ω <sub>lat</sub> (p-value)	γ <sub>IAV</sub> ( $\frac{\text{K}}{\text{ppmyr}^{-1}}$ )	γ <sub>IAV</sub> (p-value)
-	-					
R1F1L1	0.44	1.46	17.70	0.12	0.92	0.20
R1F1L2	0.99	1.88	14.69	0.57	0.95	0.23
R1F1L3	0.95	1.92	14.43	0.64	0.94	0.23
R1F2L1	0.95	1.45	17.28	0.15	0.92	0.20
R1F2L2	0.99	1.95	13.52	0.92	0.93	0.21
R1F2L3	0.94	1.97	13.55	0.91	0.92	0.21
R1F3L1	0.94	1.77	13.57	0.89	0.93	0.21
R1F3L2	0.97	2.17	9.22	0.06	0.95	0.23
R1F3L3	0.83	2.16	9.76	0.11	0.93	0.22
R1F4L1	0.85	1.44	17.91	0.10	0.91	0.20
R1F4L2	0.99	1.53	17.64	0.11	0.90	0.20
R1F4L3	0.99	1.56	17.56	0.12	0.90	0.20
R1F5L1	0.99	1.61	15.54	0.37	0.96	0.22
R1F5L2	0.98	2.11	10.97	0.29	1.01	0.27
R1F5L3	0.88	2.06	11.43	0.41	0.96	0.24
R2F1L1	0.90	1.71	15.12	0.46	0.92	0.21
R2F1L2	0.99	1.81	13.44	0.93	0.98	0.31
R2F1L3	0.95	1.89	12.66	0.80	0.95	0.28
R2F2L1	0.93	1.65	14.86	0.52	0.92	0.21
R2F2L2	0.98	1.82	12.89	0.89	0.94	0.27
R2F2L3	0.94	1.88	12.41	0.72	0.95	0.28
R2F3L1	0.93	2.07	10.63	0.24	0.94	0.23
R2F3L2	0.91	2.12	8.65	0.04	0.99	0.32
R2F3L3	0.82	2.15	8.58	0.04	0.97	0.30
R2F4L1	0.82	2.04	19.12	0.05	0.99	0.31
R2F4L2	0.98	2.12	18.28	0.08	0.98	0.31
R2F4L3	0.97	2.14	18.25	0.08	0.99	0.32
R2F5L1	0.97	2.30	16.77	0.20	0.97	0.28
R2F5L2	0.96	2.46	14.51	0.63	1.00	0.33
R2F5L3	0.94	2.47	14.55	0.62	1.00	0.34
C-only OCN	0.94	1.26	18.73	0.07	0.90	0.20
OBS	-	2.98	13.57	-	1.41	-

**Table S3.** List of stations that (wholly or partially) cover the 1982–2011 period with atmospheric CO<sub>2</sub> measurements that were used for the analysis of atmospheric constraints. Analysis of the gradient of seasonal CO<sub>2</sub> amplitudes, as presented in Fig. 1 C and D, only used northern hemispheric measurements. The station selection and observational datasets are further described by Dalmonech and Zaehle (2013).

Location	Latitude (deg)	Longitude (deg)
Alert, Canada	82.45 N	62.52 W
Point Barrow, Alaska	71.32 N	156.6 W
Station 'M', Atlantic	66 N	2 E
Cold Bay, Alaska	55.2 N	162.72 W
Shemya Island, Alaska	52.72 N	174.1 W
Mace Head, Ireland	53.33 N	9.9 W
Azores	38.75 N	27.08 W
Key Biscayne, Florida	25.67 N	80.2 W
Mauna Loa, Hawaii	19.53 N	155.58 W
Kumakahi, Hawaii	19.52 N	154.82 W
Guam	13.43 N	144.78 E
Ragged Point, Barbados	13.17 N	59.43 W
Kiritimati, Kiribati	1.7 N	157.17 W
Mahe Island, Seychelles	4.47 S	55.17 E
Ascension Island	7.92 S	14.42 W
Tutuila, American Samoa	14.25 S	170.57 W
Palmer Station, Antarctica	64.92 S	64 W
Halley Bay, Antarctica	75.67 S	25.5 W
South Pole	89.98 S	24.8 W

## References

- Dalmonech, D. and Zaehle, S.: Towards a more objective evaluation of modelled land-carbon trends using atmospheric CO<sub>2</sub> and satellite-based vegetation activity observations, *Biogeosciences*, 10, 4189–4210, 2013.
- 20 Jung, M., Reichstein, M., Margolis, H. A., Cescatti, A., Richardson, A. D., Arain, M. A., Arneth, A., Bernhofer, C., Bonal, D., Chen, J., Gianelle, D., Gobron, N., Kiely, G., Kutsch, W., Lasslop, G., Law, B. E., Lindroth, A., Merbold, L., Montagnani, L., Moors, E. J., Papale, D., Sottocornola, M., Vaccari, F., and Williams, C.: Global patterns of land-atmosphere fluxes of carbon dioxide, latent heat, and sensible heat derived from eddy covariance, satellite, and meteorological observations, *Journal of Geophysical Research*, 116, G00J07, 2011.